Influence of spatial resolution in mesoscale modeling to reproduce wind power production in southern Mexico

Article

Accepted Version

Influence of spatial resolution in mesoscale modelling to reproduce wind power production in southern Mexico

J.G. Hernández-Yepes,[1] O. Rodríguez-Hernández,[2, a)] O. Martínez-Alvarado,[3] A.V. Magaldi-Hermosillo,[4] and D. Drew[5]

[1)] *Posgrado en Ingeniería, Universidad Nacional Autónoma de México, Priv. Xochicalco s/n, Col. Centro, Temixco, Morelos, CP 62580, México*

[2)] *Instituto de Energías Renovables. Universidad Nacional Autónoma de México, Priv. Xochicalco s/n, Col. Centro, Temixco, Morelos, CP 62580, México*

[3)] *National Centre for Atmospheric Science, University of Reading, Department of Meteorology, Harry Pitt Building, Whiteknights Road, Earley Gate, Reading RG6 6ES, United Kingdom*

[4)] *ENES - Juriquilla UNAM. Universidad Nacional Autónoma de México, Querétaro, CP 76230, México*

[5)] *National Grid UK, Solihull, UK*

(Dated: 14 September 2022)

Understanding near-surface wind variability is crucial to support wind power penetration on national electrical grids. High-resolution numerical simulations are often proposed as the best solution to study the fluctuation of wind resources. We compare WRF and MERRA-2 bias-corrected wind speeds at hub height at different spatial resolutions and transform them to wind power production using a logistic power curve fitted to wind power measurements; the comparisons are based on error statistics and time series spectral analysis. Results show that numerical models reproduce observed wind speeds with correlations higher than 0.9 for WRF and 0.8 for MERRA-2. Moreover, annual observed wind power is reproduced with a maximum difference from observations of 0.011. However, each resolution reproduces the magnitudes of high-resolution periodicities differently so that there is a clear relationship between grid size and signal variance at high frequencies, as variance is indirectly proportional to frequency. This relationship is expected for wind speed but based on results it can be associated also for CF sampled at hourly intervals. Therefore, the main benefit of high spatial resolution lies in the added variance in frequencies at sub-daily timescales. The study of the added value of high-resolution simulations in this region contributes to current efforts to develop reliable forecasting tools and strategies to support the development of wind power as a reliable energy source.

Keywords: numerical resolution;capacity factor spectrum;wind power spectrum;WRF model;MERRA-2;resource assessment

I. INTRODUCTION

One of the wind energy industry's main challenges is reducing effects of wind variability on the electricity grid. Numerical atmospheric models have been used widely in the wind energy sector, playing a crucial role to understand this variability[1,2]. These models solve the Navier-Stokes equations, relating atmospheric variables with physical processes to reproduce the atmosphere's state at various spatial scales, from local to global, and for various time scales which can range between hours and centuries.

A first resource to study wind variability is provided by reanalysis data sets, typically for multidecadal periods[3]. Due to their coverage and free availability, studies have incorporated

[a)] Corresponding author: osroh@ier.unam.mx

them as a wind resource assessment mechanism. Nevertheless, a drawback that reanalyses may have is their coarse resolution, typically larger than 30 km. This characteristic limits the representation of phenomena and topographic details relevant to wind speed dynamics near the surface[4].

Limited-area mesoscale numerical weather prediction (NWP) models are models that resolve mesoscale circulations at higher spatial resolutions. Also, these models are based in the dynamical integration of the governing equations of the atmosphere. They are capable of higher levels of detail due to high resolution parameters such as orography or land use and they are intended for regional simulations. A modern approach is the use of seamless models that are capable of simulating a wide range of length and time scales, such as the UK's Met Office Unified Model (MetUM)[5]. Spatial constraints are due to the amount of computational power needed to process numerical integration at high grid resolutions. As a consequence, there is a compromise between resolution and available computational power.

A model's temporal and spatial resolution chiefly determine calculation time and computational resources demand. A number of researches use mesoscale simulations with optimal horizontal resolutions depending on the region and orography complexity. For example, Bonekamp et al.[6] simulated wind speed over the Himalayas and they got the most accurate results with 1 km and 500 m resolutions. For the UK, Drew et al.[7] investigated the effectiveness of the UKV model, with a resolution of 1.5 km, to forecast wind power rampings, and MacLeod et al.[8] used a resolution of 15 km to capture most of the small scale topographic features to reproduce wind speed and its theoretical wind power. El-Samra et al.[9] performed simulations of wind fields over Lebanon and they conclude that a 1 km grid is as precise as a 3 km grid. Additionally, a high horizontal resolution alone may not ensure the improvement of accuracy of wind speed simulations due to sensitivity of models to other parameters such as vertical resolution[10], parametrisation of the boundary layer[11], or the assimilation of observational data[12]. Thus, to optimise the process of mesoscale numerical modelling, an essential parameter to determine is the resolution of the spatial grid.

In this work, the region under study is southern Mexico, specifically the Tehuantepec Isthmus, which is surrounded by the Sierra Madre de Oaxaca, the Sierra Madre del Sur and the Sierra Madre de Chiapas (figure 1). This region is key for wind energy production in Mexico. In 2019 it concentrated 45 % of the wind power installed capacity of the country, with 2.8 GW[13]. A number of studies have given valuable knowledge for numerical modelling in this region. Olsen et al.[14] performed WRF simulations at 3 km resolution as part of the Wind Atlas of Mexico. They reported overestimations of wind speed measurements with a bias of 1.4 ms^{-1} and a correlation of 0.85 for the first months of the year. Prósper et al.[15] demonstrated that the Weather Research and Forecasting (WRF) model version 3.9[16] is able to reproduce physical phenomena in this region using high resolution simulations up to 444 m. Lira-Argüello et al.[17] used WRF (unknown version) with 1 km resolution to produce short-term forecasts of wind resources at the South of the Isthmus of Tehuantepec. Morales-Ruvalcaba et al.[18] tested NASA's Modern-Era Retrospective Analysis for Research and Applications version 2 (MERRA-2)[19] reanalysis in several regions of Mexico, being the Tehuantepec Isthmus one of them. They showed that bias corrected MERRA-2 data for this region can be highly correlated with on-site observations. More importantly, they reported an underestimation of annual variability and an overestimation of MERRA-2 derived capacity factor of 0.18 compared with real CF. Lopez-Villalobos et al.[20] reproduced the wind speed power density spectrum with measurements for the northern part of the region. They found that a mean time within 6 hours to 1 minute have no remarkable difference for annual power estimations. Also, they observed that the spectral power from MERRA-2 and the WRF model show a deviation from measurements at periods shorter than one day. However, these analyses lack two important components; first, a comparison of mesoscale simulations with real wind power production; and second, an analysis of NWP power spectrum reproducibility from wind speed conditions and power production in terms of capacity factors.

Derived from the non-linear relation of wind power and wind speed, to study the impact of numerical resolution on wind speed is not enough to understand the effects on wind power

generation. Therefore, studying directly the effects of resolution on wind power is necessary to clarify the effects and limitations on simulated energy output.

Moreover, the variability of wind speed has been studied through the mesoscale spectrum and its characterisation in numerical simulations[20–22]. For wind energy production it is known that wind energy derived from MERRA-2 reanalysis have less variability than observations, as its power spectrum underestimate frequencies above $(10\text{h})^{-1}$[23]. However, the characteristics of a capacity factor spectrum derived from mesoscale numerical models are yet to be explored in the region of our study.

Considering the aforementioned works, it is important to determine the differences and constraints when using different resolutions for wind resource assessments in the most important region in Mexico for wind power production. Therefore, the objectives of this work are to compare hourly averaged wind speed and power output of a wind turbine installed in the southern region of Mexico, with the outputs of a mesoscale model (WRF version 4)[24] and a reanalysis dataset (MERRA-2)[19] produced at different spatial resolutions (equivalent to grid spacings of 50 km for MERRA-2 and 1, 3, 15, 75 km for WRF) and to determine the amount of meaningful information in terms of wind speed and capacity factor at different grid resolutions through a power spectrum analysis.

Addressing the above mentioned objectives, the rest of the work is organised as follows: section (II) gives the characteristics and configurations about the observational data, MERRA-2 and WRF, section III presents the methodology for the analysis of data, after which results are shown in section IV, and finally, section V concludes this work.

II. DATA AND CONFIGURATIONS

Three data sets were used to develop the analysis: time series of wind observations and wind power production from a wind turbine located in Mexico's south-east region, wind speed interpolated at hub height from MERRA-2 reanalysis data, and wind speeds interpolated from WRF simulations at 1, 3, 15 and 75 km grid resolution. Details for each data set are described next.

A. Wind power data

Wind and power measurements are available from a wind turbine located in southern Mexico (due to confidentiality we are unable to give the exact location of the wind farm). The hub is at 80 meters height. The observed time series spans from 0 UTC 1 January to 2350 UTC 31 December 2016, averaged every 10 minutes. Subsequently, these time series were averaged hourly and 3-hourly for the frequency analysis (section IV C 1).

Data and the acquisition systems used in this research are continuously monitored for quality control due to their use for forecasting and wind farm operation. Missing values represent only 0.38% of total data for wind speed and 1.55% for power measurements, most of them due to instrument maintenance. To keep data quality, missing data gaps were filtered out in the time domain. In the frequency domain, time series were filled to avoid inconsistencies in observed periodicities (average of adjacent measurements, linear interpolation and WRF data). After an assessment of the impact among different completion methods, a linear interpolation was used as it showed no effects in the observed spectral power and also provided independent data to complete the time series.

B. MERRA-2 Reanalysis

The Modern-Era Retrospective Analysis for Research and Applications version 2 (MERRA-2) is the latest reanalysis developed by NASA, and the next version of the original MERRA reanalysis produced by the Global Modelling and Assimilation Office (GMAO). MERRA-2

covers from January 1980 to the present, with more than 40 data collections. The dataset that we use[25] has hourly outputs and the variables used in this work are 2-meter eastward wind (U2M), 10-meter eastward wind (U10M), eastward wind at 50 meters (U50M), 2-meter northward wind (V2M), 10-meter northward wind (V10M) and northward wind at 50 meters (V50M). These variables contain wind velocities in west-east direction (U) and south-north direction (V) over terrain height. They have a resolution of 0.5°x 0.625°, equivalent to about 55 km in latitudinal direction and 67 km in longitudinal direction for the area of study[26]. To analyse wind speed at hub height, these variables were extrapolated using the methodology detailed in section III.

C. WRF model

In this study, we use the Weather Research and Forecasting (WRF) model version 4, which is an open source atmospheric modeling system developed by the National Center for Atmospheric Research (NCAR). WRF uses the compressible, nonhydrostatic Euler equations[24], which are formulated using terrain-following hybrid pressure vertical coordinates.

WRF simulations are initialised every 24 hours and run for 30 hours, with 6 hours of spin-up, which are then discarded. This period is the minimum period reported in literature to let fine mesoscale structures to develop[22] and it is recommended from personal communications of one of the authors with Michael Duda, who is a developer of the WRF model.

The National Centers for Environmental Prediction Final Operational Global Analysis (NCEP-FNL)[27] is used as input to specify both lateral boundary conditions and initial conditions, with a horizontal resolution of 110 km approximately and 26 vertical levels. The lateral boundary conditions are ingested every 6 hours. The NCEP-FNL analysis is used as it is freely available and has been successfully tested for the same research region in the past[20].

Simulations are configured with four nested domains with mesh resolutions of 75 km, 15 km, 3 km and 1 km (figure 1), with fixed time steps of 240 s, 60 s, 20 s and 10 s respectively. Outputs are available at 10 m height and at 35 vertical levels, which include outputs at the lower levels at 26 m and 86 m height approximately. Fields are output every hour for all the domains, but the 75 km resolution domain, which has 3-hourly outputs. Table I shows the set of parametrisations used in our runs. The configuration of schemes is based on their positive performance on previous studies in this region[20].

TABLE I. WRF parametrisation setup used in this work

Parametrisation or scheme	**Reference**
Dudhia shortwave radiation	Dudhia (1989)[28]
Rapid Radiative Transfer Model for longwave radiation	Mlawer et al. (1997)[29]
WSM3 microphysical parametrisation	Hong et al. (2004)[30]
Kain-Fritsch convective parametrisation	Kain (2004)[31]
YSU planetary boundary layer scheme	Hong et al. (2006)[32]
Revised MM5 surface layer scheme	Jimenez et al. (2012)[33]
Unified Noah land surface model	Tewari et al. (2004)[34]

III. METHODOLOGY

The first step of the analysis is to evaluate the suitability of the MERRA-2 dataset and WRF model to reproduce wind speeds at hub height during 2016. To transform grided values into time series of wind speed at hub height, we assume the wind profile scales logarithmically with height. Thus, we assume that wind is a function only of surface roughness

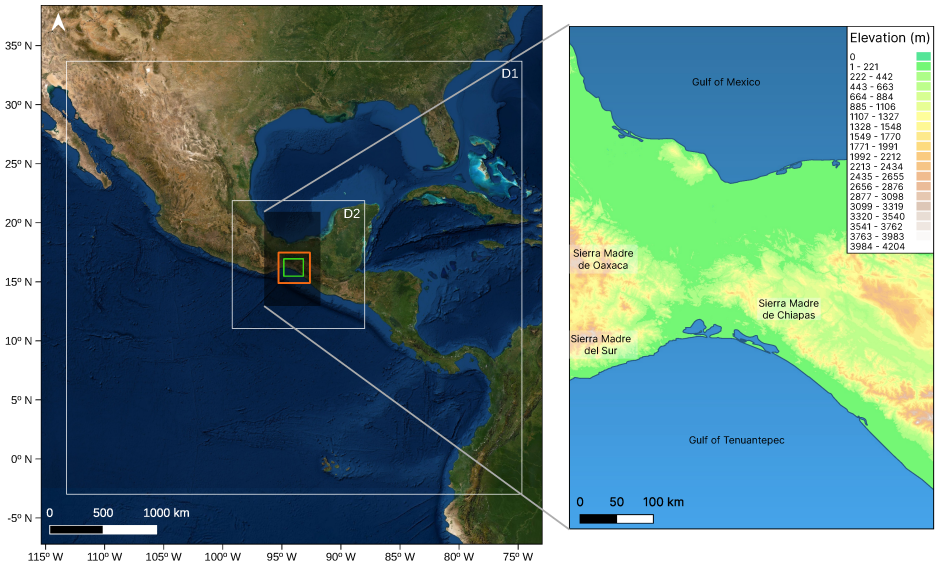

FIG. 1. Nesting of WRF domains. The green square shows domain 4 (D4) with 1 km resolution and the orange square shows domain 3 (D3) with 3 km resolution. Domain 2 (D2) has 15 km resolution and domain 1 (D1) has 75 km resolution. The zoom layer presents the location and surrounding orography of Isthmus of Tehuantepec.

without being subject to turbulence from land use changes or vegetation. Whilst this has limitations, it has been shown to be applicable under different roughness and atmospheric stability conditions[18,20,35,36].

Wind speed (U) is calculated at hub height at 80 meters (z). For WRF, a semilog-interpolation using values at 10 meters (z_1) and the second model level is used, which converted from geopotential height to geometric height is approximately at 86 meters height (z_2). Thus,

$$U = \Big(U(z_2) - U(z_1)\Big)\frac{ln(z) - ln(z_1)}{ln(z_2) - ln(z_1)} + U(z_1) \tag{1}$$

For MERRA-2 a semilog-extrapolation was performed to get hub height values from data at 2, 10 and 50 meters height above ground level.

The resulting time series, from both MERRA-2 and WRF are then bias-corrected towards observations through an empirical quantile mapping method[37] using hourly and 3-hourly time series. Using this method, nonlinear relationships between observations and modelled data can be corrected in higher detail than with linear bias correction methods[38,39]. The basis of the method is to map the distribution of observed data to the MERRA-2 or WRF distributions. For this purpose, we divide the time series into 100 quantiles and calculate a correction factor for each quantile. The corresponding correction factor used in this work is the difference between observed and modeled quantiles. Then, this correction factor is applied to each model data point according to its quantile.

Metrics used to assess model outputs are mean absolute error (MAE), mean bias (bias), root mean square error (RMSE), standard error (SE) and Pearson correlation coefficient (r):

$$MAE = \frac{1}{n}\sum_{i=0}^{n-1}|m_i - o_i|, \tag{2}$$

$$RMSE = \sqrt{\frac{1}{n}\sum_{i=0}^{n-1}(m_i - o_i)^2}, \tag{3}$$

$$SE = \frac{\sqrt{\frac{1}{n}\sum_{i=0}^{n-1}(m_i - \overline{m})^2}}{\sqrt{n}}, \tag{4}$$

$$bias = \frac{1}{n}\sum_{i=0}^{n-1}(m_i - o_i), \tag{5}$$

$$r = \frac{\sum_{i=0}^{n-1}(m_i - \overline{m})(o_i - \overline{o})}{\sqrt{\sum_{i=0}^{n-1}(m_i - \overline{m})^2}\sqrt{\sum_{i=0}^{n-1}(o_i - \overline{o})^2}}, \tag{6}$$

where n is the total samples number, m is modelled value and o is observed value.

a. Power Curve Fitting The wind turbine's theoretical power curve does assume ideal conditions that might not be met in real operations; therefore calculations using a power curve may differ, within certain error, from real power output[18]. In this work, we try to represent as accurately as possible the real performance of the wind turbine according to measurements and not according to an ideal operation. Thus, the relation between wind speed and power production is approximated using real data and the error function $erf(x) = \frac{1}{\sqrt{\pi}}\int_{-x}^{x}\exp(-t^2)dt$. The best estimate of actual performance may be calculated through modifying the coefficients of the error function, a_0, a_1, a_2 and a_3. These coefficients were computed by minimising the square of the difference between observed power and power given by the function

$$P = a_0 \cdot erf\left(\frac{U - a_1}{a_2}\right) + a_3, \tag{7}$$

where U is wind speed in ms^{-1} and P is power production in kW. The quality control described in section II ensures that the fit is not affected by wakes from adjacent wind turbines and obstacles. Additionally, we assume cut-in and cut-out wind speeds as the same as the Nordex N90/2500 turbine with recut-in at 21 ms^{-1}.

With the above considerations and based on equation 7, the best fit is as follows (figure 2):

$$P = 937.7 \cdot erf\left(\frac{U - 8.826}{4.159}\right) + 918.9 \tag{8}$$

Capacity factor (CF) is defined as the ratio of the energy production of the wind turbine to the energy that could have been produced if it operated at rated power (P_R) over a given time period (T). It is calculated as[40]:

$$CF = \frac{\sum_{i=1}^{N} P(U_i)\Delta t}{P_R T}, \tag{9}$$

where N are the data points of the time series sampled at intervals Δt.

Capacity factors are calculated using eq. 8 and 9 for each numerical dataset after bias correction. Also, CF have been calculated filtering out missing data and with the correspondent reduction in the time period (T).

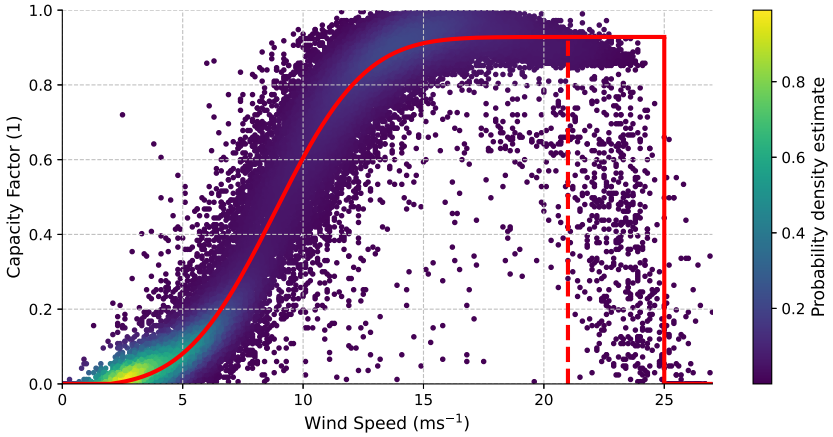

FIG. 2. Empirical power curve for the wind turbine analysed with one year of data at 10-minute resolution. The red continuous line represents the fit using the error function and the red dasshed line represents recut-in speed of 21 ms^{-1}. Shading indicates the concentration of data points.

The power curve (figure 2) reveals two clusters that represent two main states of the operation of the wind turbine. The first one is located below 0.2 and the second around 0.9 of capacity factor. The wind turbine also shows an irregular response, producing less than the rated power for wind speeds higher than 20 ms^{-1}. Hence, to fit the power curve we did not consider the values above 20 ms^{-1}.

The fitted power curve does not reach CF of 1 because it is tuned to reproduce the real conditions of operation of the wind turbine.

b. Fourier Analysis Finally, the suitability of grid sizes to reproduce different time scale processes present in wind speed or CF time series is assessed. The time series analysis variability is carried out in the frequency domain.

Power spectra S(f) are estimated through the Fast Fourier Transform and smoothed through an adaptive sine multitaper[41].

To quantify the effect of different horizontal resolutions in the reproduction of variance, a figure of merit is defined to represent the ratio of magnitude of the spectrum of observations (S_o) to the magnitude of the spectrum of models (S_m). It is applied to power spectra from diurnal time scales to the Nyquist frequency (N) as:

$$S_o : S_m = 1 - \frac{\sum_{i=(24h)^{-1}}^{N} S_{observations}(f_i)}{\sum_{i=(24h)^{-1}}^{N} S_{model}(f_i)}. \tag{10}$$

This analysis is applied to wind speed and CF with hourly and 3-hourly sampling.

IV. RESULTS AND DISCUSSION

A. Modelled wind speed

Based on the methodology described in section III WRF and MERRA-2 interpolated wind speeds were obtained at the wind turbine location and at hub height, with 3-hourly resolution for the 75 km grid and hourly for the 15, 3, 1 km grid and MERRA-2.

Table II shows that outputs from grid sizes coarser than 15 km present negative biases with respect to observations, whereas grid sizes finer than 15 km present positive biases. The 3 km grid presents the smallest errors and biases for 1 h and 3 h samplings. For the

other grids, MAE, RMSE and SE are comparable regardless of the grid size and decrease with 3 h sampling.

TABLE II. Statistic metrics of simulations of wind speed ordered by grid resolution. Metrics are calculated for hourly and 3-hourly mean times. Hourly metrics for WRF D1 data are not available because wiond speed for this grid is output only at 3-hourly resolution.

	MAE (ms^{-1})		RMSE (ms^{-1})		SE (ms^{-1})		bias (ms^{-1})		r	
Original data	1h	3h	1h	3h	1h	3h	1h	3h	1h	3h
WRF D1 - 75 km	-	2.24	-	2.79	-	0.09	-	-0.139	-	0.886
MERRA-2 $\sim$ 50 km	2.78	2.67	3.55	3.43	0.04	0.07	-1.387	-1.382	0.869	0.88
WRF D2 - 15 km	2.93	2.79	3.85	3.69	0.08	0.14	1.805	1.801	0.899	0.913
WRF D3 - 3 km	2.4	2.19	3.31	3.04	0.08	0.14	0.798	0.797	0.908	0.925
WRF D4 - 1 km	2.98	2.76	4.09	3.81	0.09	0.15	1.627	1.625	0.907	0.926
Bias corrrected data	1h	3h	1h	3h	1h	3h	1h	3h	1h	3h
WRF D1 - 75 km	-	1.89	-	2.48	-	0.11	-	-0.002	-	0.912
MERRA-2 $\sim$ 50 km	2.21	2.08	2.94	2.78	0.06	0.11	0.003	-0.008	0.88	0.891
WRF D2 - 15 km	1.98	1.81	2.6	2.38	0.06	0.11	-0.001	-0.001	0.906	0.92
WRF D3 - 3 km	1.85	1.65	2.59	2.3	0.06	0.11	-0.006	-0.005	0.906	0.924
WRF D4 - 1 km	1.84	1.62	2.59	2.26	0.06	0.11	-0.005	-0.004	0.907	0.927

Original wind speeds of WRF and MERRA-2 reproduce the bimodal distribution of observations. After bias correction, models also reproduce the bimodal distribution with a major cluster of values located under 5 ms^{-1}, and a second one near 15 ms^{-1} (figures 3A to 3J).

For all grids the overall distribution of data (red line in figures 3A to 3J) is aligned towards the identity line (black). Remarkably, the 3-hourly datasets have higher correlation coefficients than hourly data; this performance may be due to the fact that the subsampling of a time series may reduce the standard deviation in data and hence increases the correlation coefficient (table II). For the hourly averaged time series, the 15, 3 and 1 km WRF grids have similar correlation coefficients and similar least squares fit as the 75 km grid. Among those, the best are the 1 and 3 km grids and the worst is MERRA-2 grid with correlation of 0.88.

Bias correction particularly increases the ability of high resolution grids to better represent wind speed observations (figures 4A and 4B). After bias correction, the 1 km grid has the lowest MAE and RMSE (table II).

B. Wind Power Production

In this Section, wind power production is calculated from bias-corrected wind speeds and using the power curve described in section III. Specifically, we look at the ability of models to reproduce observed power production.

Models produce almost unbiased results, but with large MAE and RMSE (table III).

TABLE III. Statistic metrics of capacity factor estimations ordered by grid resolution. Metrics are calculated for hourly and 3-hourly mean times. Hourly metrics for WRF D1 data are not available because wind speed for this grid is output only at 3-hourly resolution.

	MAE (1)		RMSE (1)		SE (1)		Bias (1)	
	1h	3h	1h	3h	1h	3h	1h	3h
WRF D1 - 75 km	-	0.105	-	0.183	-	0.007	-	0.009
MERRA-2	0.126	0.121	0.222	0.208	0.004	0.007	0.01	0.009
WRF D2 - 15 km	0.11	0.102	0.195	0.177	0.004	0.007	0.008	0.007
WRF D3 - 3 km	0.105	0.095	0.193	0.17	0.004	0.007	0.011	0.009
WRF D4 - 1 km	0.105	0.095	0.194	0.169	0.004	0.007	0.009	0.008

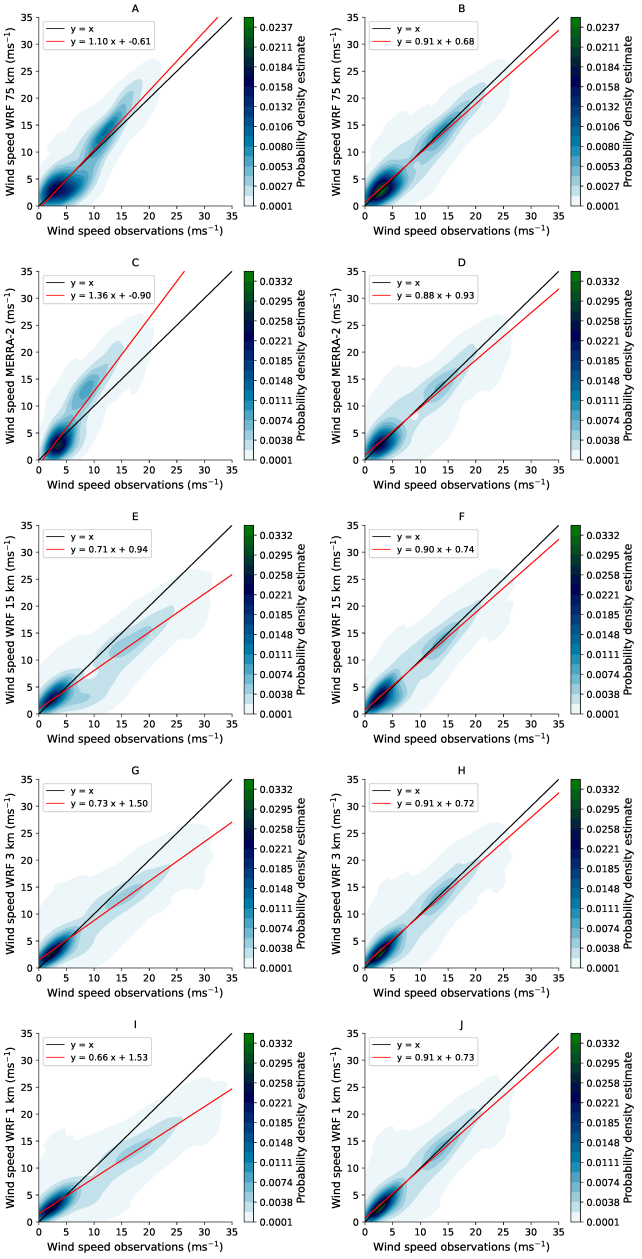

FIG. 3. Comparison of wind speed observations against wind speeds from models. Plots in the left column correspond to the relationship of observations with models' data before bias correction. Plots in the right column correspond to the relationship of observations with models' data after bias correction. Plots are ordered by grid size, thus: (A-B) WRF D1, (C-D) MERRA-2, (E-F) WRF D2, (G-H) WRF D3 and (I-J) WRF D4. The black lines indicate an identity relationship and the red lines represents a linear least squares fit to the data.

To obtain annual CF calculations were made based on hourly time series, except for the 3-hourly data of the 75 km grid. Table IV shows the contrast between real observed CF and MERRA-2 and WRF data. For observed power production: in all cases, CF is overestimated. The maximum difference is 0.012, corresponding to the 75 km WRF grid, and the minimum is for the 15 km WRF grid with 0.009.

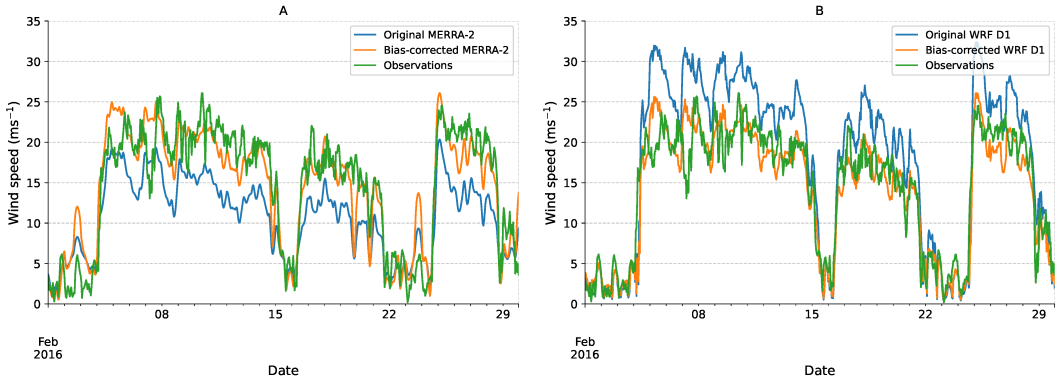

FIG. 4. Comparison of one month of models' wind speeds before and after bias correction. Original models' wind speeds are in blue, bias-corrected models' wind speeds are in orange and observations are in green. Sub-figure A presents MERRA-2 data and sub-figure B WRF D4 data.

TABLE IV. Comparison of annual capacity factor for wind power measurements and estimations from models ordered by grid size. Annual CF is calculated at hourly resolution, except for the 75 km grid at 3-hourly resolution.

Data	Annual Capacity Factor (1)
Measurements	0.33
WRF - 75 km	0.34
MERRA2 - 50 km	0.34
WRF - 15 km	0.339
WRF - 3 km	0.341
WRF - 1 km	0.339

C. Effect of horizontal resolution and sub-sampling on spectral density

1. *Hourly Wind Speed and CF*

In this section the spectral power depending on grid resolution of models is assessed.

In the first part, hourly datasets for bias corrected wind speed and capacity factor are considered and in the last part, the same datasets are used, but subsampled at 3 hours. This is to identify the added value of higher temporal resolution (section IV C 1).

The spectral power of wind speed observations presents peaks at 24 and 12 hours. The models' power spectra reproduce signal variability at the same periods as observations with an overestimation at 24 hours for WRF grids. Models introduce extra components at 8-h and 6-h periodicities that do not have physical backgrounds (figure 5A).

In terms of spectral power, the capacity factor derived from observed wind power has a similar trend as wind speed observations (figure 5B). Even though we are analysing CF, the spectral power presents a similar shape and components. This is shown by frequencies at 24-h and 12-h. For the three grids of WRF, we obtained a similar behaviour as for the wind speed spectral power: the diurnal component is enhanced.

Wind speed and CF spectral power, vary from grid to grid, with small differences in low frequencies. However, the variance of high frequencies changes with the grid in use: the finer the grid, the most spectral power in high frequencies. This is a known effect of resolution in mesoscale wind speed spectra and it can be also associated to CF spectra as results in this section suggest[20,22].

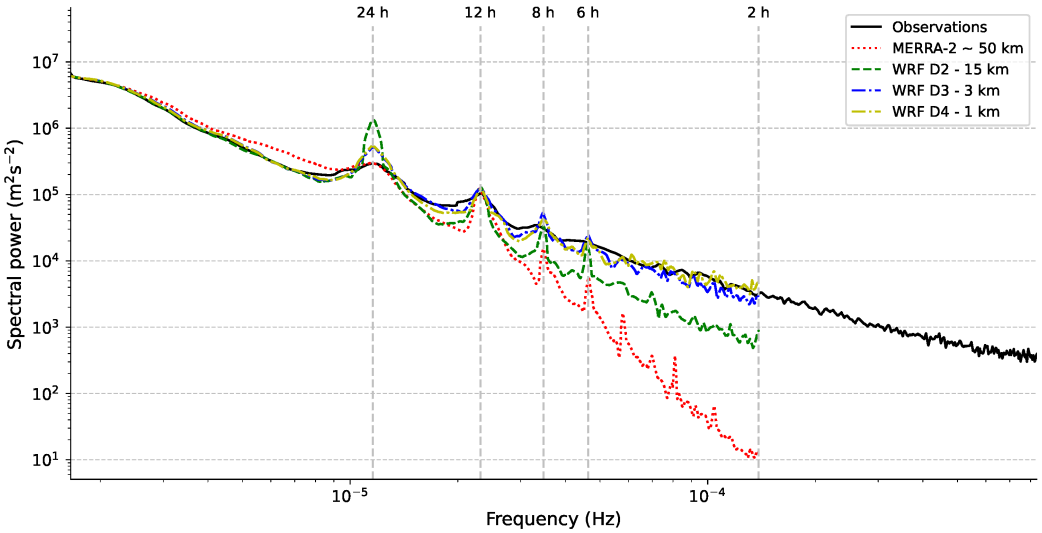

(A) Comparison of wind speed power spectra with hourly sampling.

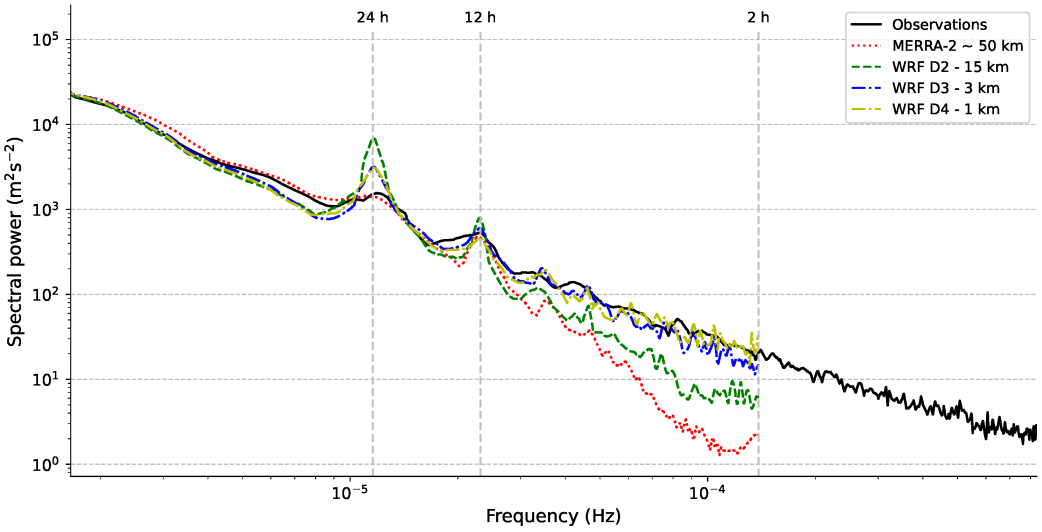

(B) Comparison of capacity factor power spectra with hourly sampling.

FIG. 5. Comparison of power spectra of wind speed (A) and CF (B) in logarithmic scale. Observations spectrum is calculated with 10 minute sampling and models spectra are calculated with hourly sampling. The dashed vertical lines indicate the inverse of relevant frequencies.

Effect of subsampling

From wind speed and CF 3-h subsampling spectral power plots were done and compared with WRF and MERRA-2 interpolations. This time, we added a new grid to the analysis, the 75 km grid of WRF, which is the largest grid size available.

The 3-hourly subsampled wind speed and CF observations produce an almost identical spectral power as their correspondent hourly data series. They also contain diurnal and semidiurnal periodicities (figures 6A and 6B). The results of the spectral power of subsampled output of models vary from grid to grid. They follow the overall distribution of power as for hourly models with frequencies at 24-h and 12-h. The differences between grids are reflected in the diverse amplitudes of the diurnal and semidiurnal periodicities and in some cases in the appearance of components that doesn't have physical mechanisms related to

them, such as the 8-hour periodicity.

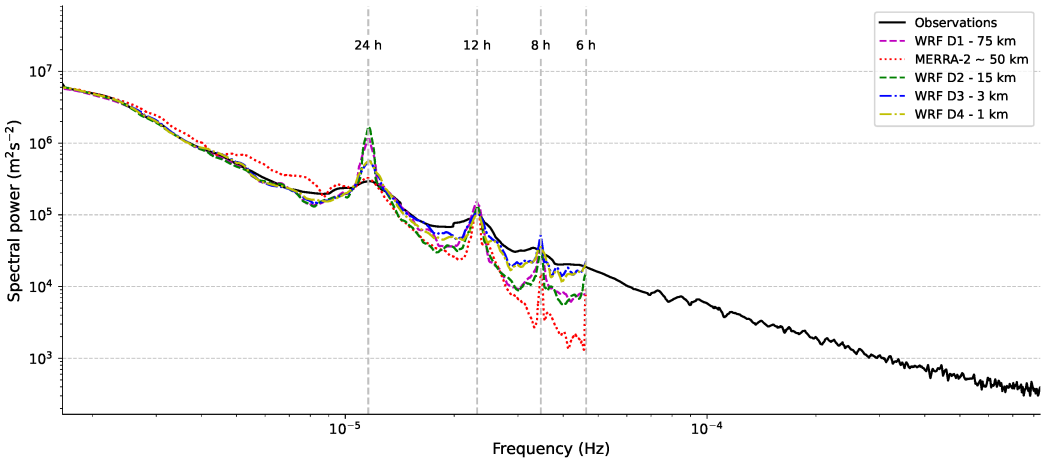

(A) Comparison of wind speed power spectra with 3-hourly sampling.

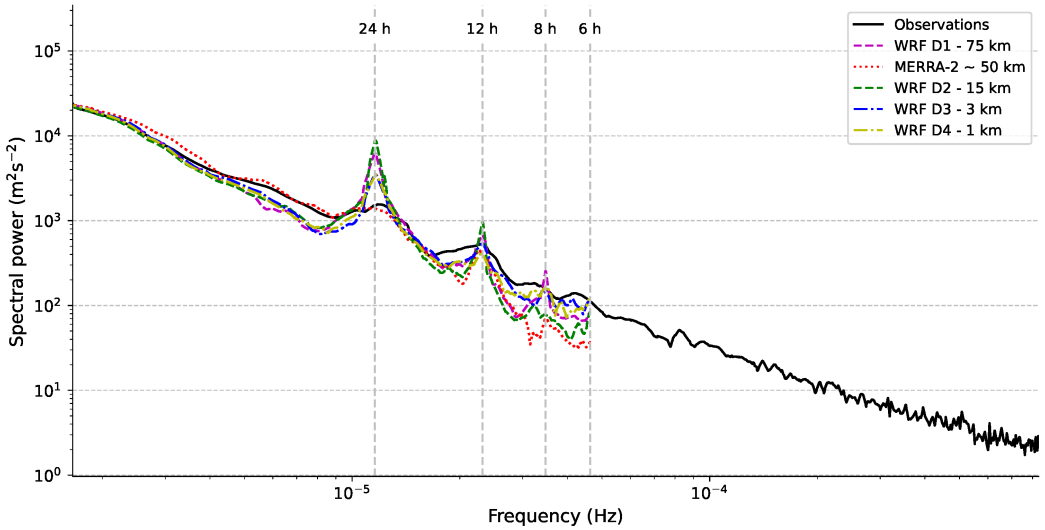

(B) Comparison of capacity factor power spectra with 3-hourly sampling.

FIG. 6. Comparison of power spectra of wind speed (A) and CF (B) in logarithmic scale. Observations spectrum is calculated with 10 minute sampling and models spectra are calculated with 3-hourly sampling. The dashed vertical lines indicate the inverse of relevant frequencies.

The results of this subsection does not show a clear relationship of variance of high frequencies with the grid in use. Specifically, as WRF D1 - 75 km spectra is comparable with finer grids spectra. Therefore, the effect of grids resolution on time series will be discussed in the next subsection.

Finally, two relevant characteristics were found in the power spectral density of wind speed and CF. The first is the fact that all grids of WRF contain higher variance at several periodicities than observed values, specially at diurnal periods (figures 5A, 5B, 6A and 6B). The overestimation of the 24 h periodicity in models spectra may be associated with the period of reinitialisation of simulations. This can be tested using other reinitialisation periods. However, too long periods can cause large deviations from analysis data. Moreover, the overestimation may not to be associated with a short spin up. Other study reported for the same region that with a 24 h period of spin-up WRF does not capture the diurnal cycle accurately (see figure 5.32 of[14]). Another possibility is the use of instantaneous WRF values

against averaged observations can be producing this effect. Whatever the cause, a deeper understanding of the reproduction of diurnal processes by WRF in the region is needed to get better simulations.

The other relevant characteristic is that the majority of the spectra of WRF grids, for wind speed and CF, introduce an artificial periodicity at 8-h and 6-h (the origin of the latter is not clear enough but may be related with the retrieving of the NCEP-FNL analysis every six hours). In both cases more research is needed to determine the source of additional variance.

2. *Ratio of spectral power*

Qualitatively, it seems that models decrease the amount of variance at sub-daily time scales as resolution decreases. To describe accurately the effect of resolution on variance, a figure of merit (9) that characterise the ratio of power spectrum of observations to models is presented (figure 7).

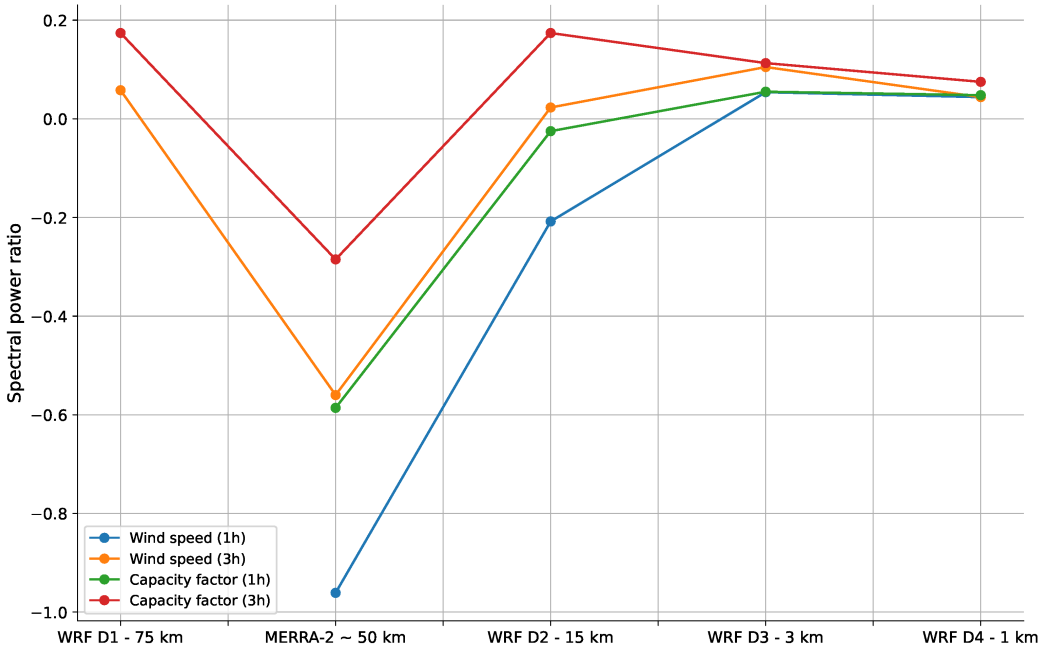

FIG. 7. Figures of merit for wind speed and CF calculated at sub-daily time scales ($(24\ \mathrm{h})^{-1}$ to the Nyquist frequency). Values above zero mean higher content of variance than observations and values below zero mean lower content of variance than observations in the specified frequency range.

Hourly time series follows the relationship between grid size and variance: as resolution increase variance increase. However, there is a saturation point at 3 km resolution and a grid of 1 km does not offer added benefits in terms of variability. As expected, MERRA-2 underestimates variance, being the resolution with the worse performance.

Three hourly time series presents a non-intuitive result for WRF at 75 km resolution. Based on the assumption that variance decreases with resolution, expected variance ratio for WRF-D1 should be minimum. However, its magnitude is comparable to all WRF grids and even greater in some cases (CF at 3 hourly resolution). The unexpected magnitudes could result of the use of instantaneous values of WRF-D1 outputs. Finer WRF grids do not follow the expected relationship between variance and resolution. This performance can be related to the limits of the Nyquist frequency ($(6\mathrm{h})^{-1}$) to reproduce measurements spectra

in high frequencies. Therefore, 3-hourly time series do not reach the range of frequencies to have a significant difference in variance reproduction.

The most consistent spatial resolutions to reproduce CF and wind speed variance across temporal scales is WRF D4 - 1 km and WRF D3 - 3 km grids. Although these spatial resolutions have similar amount of variance as observations spectra, the figure of merit should not be taken as a measurement of accuracy in specific frequencies as cancellation of peaks and valleys could lead to an apparent unbiased result.

V. CONCLUSIONS

This work analysed the suitability of NWP models to represent the wind speed and derived wind power of a wind turbine. We took as a case study a wind turbine located in southern Mexico for which we had wind speed and wind power observations. We have used MERRA-2 reanalysis and WRF model, with horizontal resolutions of 1, 3, 15, 75 km and with output every one and three hours, to investigate the influence of the spatio-temporal resolution on the representations of wind speed and wind power production. Evaluations were made using MAE, RMSE, SE, bias, correlation and a frequency spectrum analysis of wind speed and CF.

Wind speed for 2016 has a bimodal distribution and models' outputs are able to reproduce it with several differences depending on the grid size. For the raw outputs of WRF model at hourly resolution, the 3 km grid has the most accurate reproduction and as the grid size increases, the correlation slightly decreases. Results suggest that with the current configuration there could be an improvement in the bias and correlation of wind speed in the region compared with previous studies. Additionally, even if models have deviations from reality, with a statistical correction they can significantly increase their performance: after bias correction all the grids of WRF have small error statistics.

In the process to estimate wind power production from wind speed data, the power curve is a key factor as it should correctly represent the performance of a wind turbine. To fit an error function as a power curve showed a good approximation for the wind turbine analysed, as we were able to reproduce the annual CF with a maximum difference of 0.01. Although the power curve fit produces a small bias for annual CF calculations, for shorter time scales it may not necessarily reflect CF accurately as high values of MAE and RMSE demonstrate.

Results show that WRF reproduce variance at high frequencies up to different ranges. For hourly time series grids of 3 km and 1 km resolution can provide the best level of detail of the wind speed dynamics. However, the 3 km grid provides an optimal balance between detailed wind dynamics and the computational time needed to reproduce it. Therefore, using a 1 km resolution may not be worth the computational resources.

In essence, the added value of high numerical resolutions in this important region of Mexico for wind energy is the reproduction of variance at daily and sub-daily scales of wind speed and CF at hourly resolutions. Modelled values at 3-hourly resolution are not able to reproduce the spectra beyond $(6\text{h})^{-1}$ and they reproduce incompletely the high frequencies present in original time series. Thus, hourly mesoscale simulations in the Isthmus of Tehuantepec region can be used as a tool to reproduce fine details not present in global reanalyses and coarse grids. However, our results also confirm that there is room for improvement in the accuracy of WRF to reproduce the diurnal cycle. Further optimisation of mesoscale parameters could help to get accurate daily forecasts for predicting extreme events, such as ramping, and assist in the short-term management of wind farms. Similarly, accurate daily forecasts can be effective for the grid operator to balance power production with load.

ACKNOWLEDGEMENTS

The contributions and publishing of this paper were supported by Mexico CONACYT-SENER Sustentabilidad Energética, Project 272063, Strengthening of the field of Wind Energy in the Doctoral Program in Engineering Field of Knowledge in Energy based in the Institute of Renewable Energies of the National Autonomous University of Mexico; (Institutional Strengthening for Energy Sustainability).

This work was done during José Gustavo Hernández-Yepes Master's studies at IER UNAM, which were funded by CONACYT Beca de Posgrado Nacional FSE-SENER-CONACyT from 2017 to 2019.

Part of this research was done during a research stay of José Gustavo Hernández-Yepes at The University of Reading, United Kingdom from September to December 2018, which was funded by UNAM Programa de Apoyo a los Estudios de Posgrado (PAEP) and Project 272063.

Figure 1 was produced using GIS4WRF[42,43].

DATA AVAILABILITY STATEMENT

The data that support the findings of this study are available from private sector. Restrictions apply to the availability of these data, which were used under license for this study. Data are available from the authors upon reasonable request and with the permission of the data provider.

[1]S. Al-Yahyai, Y. Charabi, and A. Gastli, "Review of the use of Numerical Weather Prediction (NWP) Models for wind energy assessment," Renewable and Sustainable Energy Reviews **14**, 3192–3198 (2010).

[2]P. Veers, K. Dykes, E. Lantz, S. Barth, C. L. Bottasso, O. Carlson, A. Clifton, J. Green, P. Green, H. Holttinen, D. Laird, V. Lehtomäki, J. K. Lundquist, J. Manwell, M. Marquis, C. Meneveau, P. Moriarty, X. Munduate, M. Muskulus, J. Naughton, L. Pao, J. Paquette, J. Peinke, A. Robertson, J. Sanz Rodrigo, A. M. Sempreviva, J. C. Smith, A. Tuohy, and R. Wiser, "Grand challenges in the science of wind energy," Science **366**, eaau2027 (2019).

[3]D. Dee, J. Fasullo, D. Shea, J. Walsh, and National Center for Atmospheric Research Staff, "The Climate Data Guide: Atmospheric Reanalysis: Overview & Comparison Tables," (2016).

[4]I. Staffell and S. Pfenninger, "Using bias-corrected reanalysis to simulate current and future wind power output," Energy **114**, 1224–1239 (2016).

[5]D. N. Walters, M. J. Best, A. C. Bushell, D. Copsey, J. M. Edwards, P. D. Falloon, C. M. Harris, A. P. Lock, J. C. Manners, C. J. Morcrette, M. J. Roberts, R. A. Stratton, S. Webster, J. M. Wilkinson, M. R. Willett, I. A. Boutle, P. D. Earnshaw, P. G. Hill, C. MacLachlan, G. M. Martin, W. Moufouma-Okia, M. D. Palmer, J. C. Petch, G. G. Rooney, A. A. Scaife, and K. D. Williams, "The Met Office Unified Model Global Atmosphere 3.0/3.1 and JULES Global Land 3.0/3.1 configurations," Geoscientific Model Development **4**, 919–941 (2011).

[6]P. N. J. Bonekamp, E. Collier, and W. W. Immerzeel, "The Impact of Spatial Resolution, Land Use, and Spinup Time on Resolving Spatial Precipitation Patterns in the Himalayas," Journal of Hydrometeorology **19**, 1565–1581 (2018).

[7]D. R. Drew, D. J. Cannon, J. F. Barlow, P. J. Coker, and T. H. Frame, "The importance of forecasting regional wind power ramping: A case study for the UK," Renewable Energy **114**, 1201–1208 (2017).

[8]D. MacLeod, V. Torralba, M. Davis, and F. Doblas-Reyes, "Transforming climate model output to forecasts of wind power production: How much resolution is enough?: Transforming climate model output to wind power forecasts," Meteorological Applications **25**, 1–10 (2018).

[9]R. El-Samra, E. Bou-Zeid, and M. El-Fadel, "What model resolution is required in climatological downscaling over complex terrain?" Atmospheric Research **203**, 68–82 (2018).

[10]E. N. Smith, J. A. Gibbs, E. Fedorovich, and P. M. Klein, "WRF Model Study of the Great Plains Low-Level Jet: Effects of Grid Spacing and Boundary Layer Parameterization," Journal of Applied Meteorology and Climatology **57**, 2375–2397 (2018).

[11]D. Siuta, G. West, and R. Stull, "WRF Hub-Height Wind Forecast Sensitivity to PBL Scheme, Grid Length, and Initial Condition Choice in Complex Terrain," Weather and Forecasting **32**, 493–509 (2017).

[12]L. Giovannini, G. Antonacci, D. Zardi, L. Laiti, and L. Panziera, "Sensitivity of Simulated Wind Speed to Spatial Resolution over Complex Terrain," Energy Procedia **59**, 323–329 (2014).

[13]Asociación Mexicana de Energía Eólica, "Mapa Eólico," https://amdee.org/mapas-eolicos.html (2019).

[14]B. T. Olsen, A. N. Hahmann, D. Cavar, A. Peña, H. Villanueva, N. N. Davis, and J. C. Hansen, "Mesoscale and microscale downscaling for the Wind Atlas of Mexico (WAM) project," DTU Wind Energy DTU Wind Energy E, 77.

[15]M. A. Prósper, I. Sosa Tinoco, C. Otero-Casal, and G. Miguez-Macho, "Downslope windstorms in the Isthmus of Tehuantepec during Tehuantepecer events: A numerical study with WRF high-resolution simulations," Earth System Dynamics **10**, 485–499 (2019).

[16]W. Skamarock, J. Klemp, J. Dudhia, D. Gill, D. Barker, W. Wang, X.-Y. Huang, and M. Duda, "A Description of the Advanced Research WRF Version 3," Tech. Rep. (UCAR/NCAR, 2008).

[17]R. Lira-Argüello, M. A. Ruiz-Jaimes, U. M. Miranda, S. Flores, O. Díaz-Parra, A. Fuentes-Penna, and Y. Toledo-Navarro, "Forecast of the Wind Speed using the Regional Atmospheric Modeling System (RAMS) and Weather Research and Forecasting (WRF) models," International Journal of Combinatorial Optimization Problems and Informatics **9**, 14 (2018).

[18]C. Morales-Ruvalcaba, O. Rodríguez-Hernández, O. Martínez-Alvarado, D. Drew, and E. Ramos, "Estimating wind speed and capacity factors in Mexico using reanalysis data," Energy for Sustainable Development **58**, 158–166 (2020).

[19]R. Gelaro, W. McCarty, M. J. Suárez, R. Todling, A. Molod, L. Takacs, C. A. Randles, A. Darmenov, M. G. Bosilovich, R. Reichle, K. Wargan, L. Coy, R. Cullather, C. Draper, S. Akella, V. Buchard, A. Conaty, A. M. da Silva, W. Gu, G.-K. Kim, R. Koster, R. Lucchesi, D. Merkova, J. E. Nielsen, G. Partyka, S. Pawson, W. Putman, M. Rienecker, S. D. Schubert, M. Sienkiewicz, and B. Zhao, "The Modern-Era Retrospective Analysis for Research and Applications, Version 2 (MERRA-2)," Journal of Climate **30**, 5419–5454 (2017).

[20]C. Lopez-Villalobos, O. Rodriguez-Hernandez, O. Martínez-Alvarado, and J. Hernandez-Yepes, "Effects of wind power spectrum analysis over resource assessment," Renewable Energy **167**, 761–773 (2020).

[21]X. G. Larsén, S. E. Larsen, and E. L. Petersen, "Full-Scale Spectrum of Boundary-Layer Winds," Boundary-Layer Meteorology **159**, 349–371 (2016).

[22]W. C. Skamarock, "Evaluating Mesoscale NWP Models Using Kinetic Energy Spectra," Monthly Weather Review **132**, 3019–3032 (2004).

[23]J. Olauson, H. Bergström, and M. Bergkvist, "Restoring the missing high-frequency fluctuations in a wind power model based on reanalysis data," Renewable Energy **96**, 784–791 (2016).

[24]W. C. Skamarock, J. B. Klemp, J. Dudhia, D. O. Gill, Z. Liu, J. Berner, W. Wang, J. G. Powers, M. G. Duda, D. M. Barker, and X.-Y. Huang, "A Description of the Advanced Research WRF Model Version 4," Tech. Rep. (National Center for Atmospheric Research, 2019).

[25]Global Modeling and Assimilation Office (GMAO), "MERRA-2 tavg1_2d_slv_Nx: 2d,1-Hourly,Time-Averaged,Single-Level,Assimilation,Single-Level Diagnostics V5.12.4," (2015).

[26]M. G. Bosilovich, R. Lucchesi, and M. Suarez, "MERRA-2: File Specification," Tech. Rep. (GMAO Office Note No. 9 (Version 1.1), 2016).

[27]"NCEP FNL Operational Model Global Tropospheric Analyses, continuing from July 1999," (2000).

[28]J. Dudhia, "Numerical study of convection observed during the winter monsoon experiment using a mesoscale two-dimensional model," Journal of Atmospheric Sciences **46**, 3077–3107 (1989).

[29]E. J. Mlawer, S. J. Taubman, P. D. Brown, M. J. Iacono, and S. A. Clough, "Radiative transfer for inhomogeneous atmospheres: RRTM, a validated correlated-k model for the longwave," Journal of Geophysical Research: Atmospheres **102**, 16663–16682 (1997).

[30]S.-Y. Hong, J. Dudhia, and S.-H. Chen, "A Revised Approach to Ice Microphysical Processes for the Bulk Parameterization of Clouds and Precipitation," MONTHLY WEATHER REVIEW **132**, 18 (2004).

[31]J. S. Kain, "The Kain–Fritsch Convective Parameterization: An Update," JOURNAL OF APPLIED METEOROLOGY **43**, 12 (2004).

[32]S.-Y. Hong, Y. Noh, and J. Dudhia, "A New Vertical Diffusion Package with an Explicit Treatment of Entrainment Processes," Monthly Weather Review **134**, 2318–2341 (2006).

[33]P. A. Jiménez, J. Dudhia, J. F. González-Rouco, J. Navarro, J. P. Montávez, and E. García-Bustamante, "A Revised Scheme for the WRF Surface Layer Formulation," Monthly Weather Review **140**, 898–918 (2012).

[34]M. Tewari, F. Chen, W. Wang, J. Dudhia, M. A. LeMone, G. Gayno, J. Wegiel, and R. H. Cuenca, "Implementation and verification of the Unified Noah Land Surface Model in the WRF model," in *20th Conference on Weather Analysis and Forecasting/16th Conference on Numerical Weather Prediction* (2004) pp. 11–15.

[35]D. Cannon, D. Brayshaw, J. Methven, P. Coker, and D. Lenaghan, "Using reanalysis data to quantify extreme wind power generation statistics: A 33 year case study in Great Britain," Renewable Energy **75**, 767–778 (2015).

[36]C. W. Kent, C. Grimmond, D. Gatey, and J. F. Barlow, "Assessing methods to extrapolate the vertical wind-speed profile from surface observations in a city centre during strong winds," Journal of Wind Engineering and Industrial Aerodynamics **173**, 100–111 (2018).

[37]T. Lafon, S. Dadson, G. Buys, and C. Prudhomme, "Bias correction of daily precipitation simulated by a regional climate model: A comparison of methods: BIAS CORRECTION OF DAILY PRECIPITATION SIMULATED BY A REGIONAL CLIMATE MODEL," International Journal of Climatology **33**, 1367–1381 (2013).

[38]D. Li, J. Feng, Z. Xu, B. Yin, H. Shi, and J. Qi, "Statistical Bias Correction for Simulated Wind Speeds Over CORDEX-East Asia," Earth and Space Science **6**, 200–211 (2019).

[39]S. R. Thomas, O. Martínez-Alvarado, D. Drew, and H. Bloomfield, "Drivers of extreme wind events in Mexico for windpower applications," International Journal of Climatology , joc.6848 (2020).

[40]J. F. Manwell, J. G. McGowan, and A. L. Rogers, *Wind Energy Explained: Theory, Design and Application* (John Wiley & Sons Ltd, 2009).
[41]G. A. Prieto, "The *Multitaper* Spectrum Analysis Package in Python," Seismological Research Letters **93**, 1922–1929 (2022).
[42]D. Meyer and M. Riechert, "Open source QGIS toolkit for the Advanced Research WRF modelling system," Environmental Modelling & Software **112**, 166–178 (2019).
[43]D. Meyer and M. Riechert, "The GIS4WRF Plugin," Zenodo (2020).